Pervaporative Denitrogenation of Pyrrole/*n*-heptane as Model Oil using MoO_3 -PEBAX/PAN membrane

Kun Liu
Guangxi University College of Chemistry and Chemical Engineering
Qiu-Lan Yu
Guangxi University College of Chemistry and Chemical Engineering
Yaseen Muhammad (myyousafzai@gmail.com)
University of Peshawar
Sidra Subhan
Institute of Chemical Sciences, University of Peshawar

Research Article

Keywords: MoO3/PEBAX membrane, Pervaporation, Pyrrole/n-heptane mixture separation, textural characterization, denitrogenation of fuel oil.

Posted Date: May 6th, 2021

DOI: https://doi.org/10.21203/rs.3.rs-400503/v1

Abstract

The environmentally obnoxious nature of Nitrogen in fuel oils requires serious attention for its removal. In this work, a novel hybrid matrix membrane was prepared by introducing MoO_3 nanoparticles into poly (ether-block-amide) (PEBAX2533) and was in turn used for the pervaporative separation of pyrrole/*n*-heptane mixtures. The interactions between the membrane, pyrrole and *n*-heptane were investigated by swelling experiments. Pervaporative separation performance of PEBAX membranes revealed higher selectivity for pyrrole from its mixture with *n*-heptane, which further increased with increasing MoO_3 contents in membrane along-with correspondingly increasing the total flux and the separation factor as well. At 2000 $\mu g \cdot g^{-1}$ pyrrole concentration and 30°C temperature, the total flux and the separation factor reached the maximum values of 2.46 $kg \bullet m^{-2} \bullet h^{-1}$ and 17.58, respectively. Attributed to the outstanding separation performance of PEBAX membranes, this work may provide a useful insight into the viable removal of nitrogenous compounds from gasoline via pervaporation.

1. Introduction

Due to the increasingly stringent environmental regulations regarding the quality of transportation fuels, ultra-low sulfur, nitrogen, and aromatics containing fuels are highly demanded (Busca &Research 2009, Mojaverian Kermani et al. 2018, Muhammad et al. 2019a, Muhammad et al. 2019b). These species lead to the production of NO_x, SO_x, CO and CO_2 as major pollution contributors upon combustion of fuel oils (Ali et al. 2006, Rahman et al. 2018, Subhan et al. 2019a, Subhan et al. 2019b). Among these, nitrogenous compounds such as indole and carbazole are more stable having lower activity than sulfur compounds, and hence their removal via hydrodenitrification (HDN) is a challenging task (Oliveira et al. 2004). In addition, these nitrogenous compounds also detrimentally affects the efficiency the industrial various desulfurization processes (Ammar et al. 2020, Laredo et al. 2015, Nunes et al. 2014). Along with their stability, neutral nitrides are easily converted into basic nitrides which then compete with sulfur compounds for active sites of catalysts, causing catalyst deactivation and ultimately reduce catalyst service life (Dorbon &Bernasconi 1989). Apart from this, combustion of these nitrogenous compounds leads to NO_X production which in turn trigger acid rain endangering biotic as well as abiotic segments of ecosystem (Abdul-quadir et al. 2018, Marani et al. 2017, Sun et al. 2018). In addition to acid rain, NO_X also lead to photochemical pollution and haze and depletion of ozone layer. In combination to NOx production, some of the neutral nitrides in fuel oils like indoles can go through oligomerization during hydrogenation catalysis, can corrode equipment and interfere and deteriorate the stability of refined products through gum formation and altering color and odor (Adams et al. 1984, McKay et al. 1976). Awarding to these aspects, it is significantly desired to remove basic nitrogen compounds for optimizing the fluid catalytic cracking (FCC) process and improving the quality of light fuels.

The removal of nitrogen compounds from gasoline is mainly achieved by HDN utilizing a metal oxide/sulfide-based catalyst and zeolites (Escola et al. 2012, Li et al. 2009, Mapiour et al. 2010, Yu et al. 2010). However, due to high operating temperatures and pressures, HDN requires exorbitant devices, high

hydrogen consumption, high production cost, and reduced heptane number of the final gasoline. On the contrary, pervaporation is a promising and effective technique for the removal of nitrogen attributed to its low operating cost, high separation efficiency, simplified operation procedure, and adaptability to changes in processing streams (Mortaheb et al. 2012).

Pyrrole is major nitrogen compound in FCC gasoline. The solubility parameter is the square root of cohesive energy per molar volume and is calculated by group contribution method (Balko et al. 2002). The solubility parameters of pyrrole, *n*-heptane and Poly (ether-block-amide) (PEBAX2533) are 19.5 $J^{1/2}•cm^{-3/2}$,15.3 $J^{1/2}•cm^{-3/2}$ and 19.1 $J^{1/2}•cm^{-3/2}$ respectively, suggesting similar solubility parameters of pyrrole and polymeric material than *n*-heptane. PEBAX2533 are comprised by a series of block copolymers of flexible polyether (PE) and blocks of rigid polyamide (PA) (Lin et al. 2006). PEBAX copolymer possesses high mechanical strength and toughness with high concentration of PA chain segments, thus improving the ratio of PE chain segments in PEBAX which can award the polymer with better affinity to organic compounds (Lin et al. 2006). Among these, PEBAX2533 contain the highest concentration of PE, and is deemed a promising membrane material due to its high hydrophobicity, remarkable physical and mechanical strength, and good thermal stability, has been ubiquitously applied in separation of aromatic compounds (Gao et al. 2020, Lin et al. 2008, Lin et al. 2009). Kun Liu et al. separated mixture of thiophene/*n*-heptane using PEBAX/PVDF-composited membranes and PEBAX membrane for the separation of *n*-butyl acetate, *n*-butanol, and acetic acid from aqueous solutions via pervaporation (Liu et al. 2013). Similarly, Ding He et al. reported enhanced desulfurization performance and stability of PEBAX membrane (Amaral et al. 2014, Huang et al. 2020, Song et al. 2020). Fusheng Pan et al. embedded Ag^{+}@COFs into PEBAX membrane to construct mass transport channels which elevated desulfurization performance (Le et al. 2011).

To our knowledge, no reports on the pervaporative removal of pyrrole from gasoline using composite PEBAX membranes have been established yet. These type of membranes with dense active layer covered on a porous supporting layer, have been extensively adopted in commercial pervaporation process endorsed to their enhanced mechanical properties, resistance to corrosion and swelling (Yildirim et al. 2008). This type of interaction can synchronously enhance permeating flux and selectivity of composite membrane. In this connection, mixed matrix membranes, composed of efficient activated adsorption fillers dispersed in a polymeric matrix have been reported with enhanced pervaporation performance (Castro-Muñoz 2019, Merkel et al. 2013). Among the many adsorbent, MoO_3 has been proved nitrogen-selective (specially preferential retaining efficiency for pyrrole) from its mixture with other organic compounds (Chen et al. 2010, Huang &Meagher 2001). Thus, herein we report a MoO_3 microspheres introduced PEBAX polymer to obtain MoO_3 filled PEBAX Polyacrylonitrile (PEBAX/PAN) membrane and in turn apply it for the pervaporative removal of pyrrole from *n*-heptane as model gasoline. The structure morphology of MoO_3 microspheres and hybrid membranes were characterized by scanning electron microscopy (SEM), while MoO_3 concentration, temperature and pyrrole concentration of feed were systematically evaluated affecting the separation performance of membrane in the swelling and pervaporation experiments.

2. Experimental

2.1. Materials

PEBAX2533 was supplied by Arkema Inc. PAN ultrafiltration membrane with a molecular weight cut-off of 5 kDa was purchased from Shanghai Lanjing membrane & engineering Co. Ltd. *N*-heptane, *n*-butanol, ethyl alcohol and *n*-propanol were provided by Guangdong xilong chemicals Inc. Guangdong China. Pyrrole and MoO_3 were purchased from Aladdin Inc. China. All reagents were of analytical grade and used without further purification. Deionized water was used throughout the experiments where required.

2.2. Preparation of membranes

2.2.1 Preparation of PEBAX homogeneous membrane and MoO_3 filled membrane

PEBAX 2533 particles were dried to constant weight in an oven at 50 ^{o}C, and were then dissolved in a conical bottle containing certain amount of *n*-butanol. The mixture was heated to 50 ^{o}C in a water bath and stirred for 1 h till the formation of homogeneous solution representing 7 wt.% transparent polymer casting solution. This solution was vacuumed for 0.5 h to remove bubbles and was evenly poured onto the clean and flat glass plate to form a uniform film. The solvent was evaporated by heating in a dust-free environment for 24 h, and was then dried thoroughly in a vacuum drier at 50 ^{o}C. The film was stored in a dryer for using.

To prepare the filled film, 7 wt.% casting solution was made by the same method, followed by the addition of nano MoO_3 equivalent to 2 wt.%, 4 wt.%, 6 wt.% and 8 wt.% of the mass of PEBAX2533 particles. The casting solution was dissolved and stirred for 2 h at 70 ^{o}C followed by ultrasonication for 10 min. The solution was once again stirred for 1 h to enhance the dispersion of MoO_3. Finally, the solution was allowed static under vacuum for 30 min to remove any trapped air bubbles.

2.2.2 Preparation of PEBAX/PAN composite membrane and nano MoO_3 filled- composite membrane

Composite membrane was prepared by treating PAN supporting membrane with anhydrous ethanol and was fixed on a clean and dry glass plate. When the membrane was semi-wet, the casting solution was evenly dumped into the middle of the membrane, and was then scraped. The treatment and preservation steps were similar as those mentioned for the preparation of homogeneous membrane.

Filled-composite membrane was prepared by the above-mentioned nano MoO_3 filled casting membrane with different filling ratios followed by scraping it on the PAN support membrane. The treatment and preservation steps were again similar to those mentioned for the preparation of filled membrane.

2.3. Characterization of membranes

The morphology of MoO_3 microspheres was observed by SEM (Hitachi S3400, Japan). The pore size of PAN film was measured by Aperture analyzer. Membrane samples were fractured in liquid nitrogen and

then analyzed for surface morphology and dispersion of MoO_3 microspheres by SEM. Fourier transform infrared (FT-IR, 8400S, Japan) spectra and X-ray diffraction (XRD, TD-2500, China) were used to determine the chemical composition and crystallite size of the microspheres, respectively.

2.4 Swelling experiments

A cut piece of membrane was dried in a vacuum oven at 50 ^{o}C for 48 h until constant mass. It was then immersed in the feed mixture for 5 min and removed with a forceps and wiped with filter paper to remove the surface mixture following by weighing it. Each experiment was performed in triplicates and average values were recorded. Films dried until constant mass were placed in weighing bottles to weigh then recorded as W_d. Under dry environment, films were immersed in capacity bottles containing 40 mL pyrrole/*n*-heptane with different pyrrole concentration. Films were heated by water bath pot according to different temperatures. The residual liquid on film surface was sponged with filter papers. The weight of the wet films was recorded as Ws. The swelling experiments were repeated three times, and average values were reported . The degree of swelling (DS) was calculated using **Eq. (1)** (Qu et al. 2010):

$$DS(\%) = \frac{W_w - W_d}{W_d} \times 100 \qquad (1)$$

The main contents of swelling experiment were as follows: the relationship between DS and time of filled film was investigated, when the pyrrole concentration in feed liquid was 0, 1000 μg·g^{-1}, 2000 μg·g^{-1}, 3000 μg·g^{-1}, 4000 μg·g^{-1}, 5000 μg·g^{-1}, respectively and at 30 ^{o}C feed temperature, the relationship between temperature and swelling performance of filled films was investigated.

2.5. Pervaporation experiments

The schematic of the pervaporation apparatus is shown in **Fig. 1** (Sampranpiboon et al. 2000). The liquid circulation system consists of temperature controller, liquid tank and diaphragm circulating pump. The effective membrane area of membrane module customized by Zhejiang University is 19.63 cm^2. The feed liquid is pumped from the circulating pump to membrane tank at atmospheric upstream pressure, while that of the downstream was maintained at approximately -100 kPa by a vacuum pump. Interception fluid is returned to the liquid tank for continuous circulation, and osmotic fluid is collected by condensing in liquid nitrogen (-196 ^{o}C). Samples were collected twice per hour in three parallel experiments.

Permeation total flux refers to the quality of feed liquid passing through membrane of unit area per unit time, which reflects the capacity of membrane to treat feed liquid and is calculated via **Eq. (2)** (Sampranpiboon et al. 2000):

$$J = \frac{M}{A \times t} \qquad (2)$$

Here J is the total permeation flux ($kgm^{-2}h^{-1}$), M and A refer to mass of the osmotic fluid (g) and effective area of membrane (m^2), respectively, and t is Penetration time.

Separation factor refers to the ratio of pyrrole concentration in osmotic fluid and raw feed liquid, which reflects the Separation selectivity of membrane, and is calculated using **Eq. (3)**:

$$\alpha = \frac{y_1/y_2}{x_1/x_2} \quad (3)$$

Where a is the separation factor, y_1 and y_2 refer to the mass fractions of pyrrole and n-heptane in feed liquid, respectively, and x_1 and x_2 are the mass fractions of pyrrole and n-heptane, respectively.

Pervaporation separation index is used as a characterization parameter for the comprehensive performance of pervaporation membrane and is measured using **Eq. (4)** (Zi 1996):

$$PSI = J \times (\alpha - 1) \quad (4)$$

Where, PSI is pervaporation separation index, J is the permeation flux ($kgm^{-2}h^{-1}$), and 'a' is the separation factor.

3. Results And Discussion

3.1 Textural characterization of membranes

The appearances of MoO_3 microspheres detected by SEM shown in **Fig. 2a** revealed their inerratic sphericity, with fairly uniform distributions having a diameter of about 200 nm.

3.1.1 Morphology of membranes

The structure of composite membrane and filled composite membrane was investigated by SEM. **Fig. 2b** showcasing the surface of the composite membrane suggests pyknotic, imperforated and flawless PEBAX2533 active layer. **Fig. 2c** manifested well monodispersed MoO_3 microspheres in PEBAX2533 layer without any aggregation. The filling amount of MoO_3 microspheres in the filled composite membrane was selected as 4 wt.% (due to its best performance of swelling and pervaporation to be discussed in the proceeding sections of the manuscript). The cross-sectional SEM images of the composite membrane and filled composite membrane shown in **Fig. 2d** and **2e**, respectively, suggested a dense PEBAX2533 active layer with a uniform thickness of about 22 µm, firmly adhered on the PAN support without any blemishes, which confirmed the uniform dispersion of MoO_3 particles. The interface between the two

layers was properly interconnected, while PEBAX2533 polymer solution did not penetrate into the PAN support

3.1.2 FT-IR analysis of microspheres

The FT-IR results of composite membrane and composite-filled membrane shown in **Fig. 3** indicated peaks at 723 cm^{-1} and 1100 cm^{-1} ascribed to characteristic stretching-vibration of -CH_2-CH_2-CH_2- bond and the band of -C-O- in polyether of PEBAX, respectively (Liu et al. 2013). Peak at 1740 cm-1 was caused by the stretching vibration of -C=O- double bond in polyamide, while the one at 3294.19 cm^{-1} was awarded to the characteristic stretching vibration of -NH- in polyamide (Wu &Xu). Furthermore, the FTIR spectra of the composite membrane was very much identical to that of the filled-composite membrane, without the appearance of new functionalities, which suggested that MoO_3 particles physically filled into the PEBAX2533 active layer.

3.1.3 XRD analysis of the microspheres

The XRD patterns of MoO_3 particles, composite membrane, and composite-filled membrane are shown in **Fig. 4**. The smaller diagram in the right upper shows the spectrum of MoO_3. The spectra of composite membrane and composite-filled membrane are basically the same, and only a wide diffraction peak appears in the range of 12^o~35^o, which suggested the amorphous nature of PEBAX2533 membrane, while MoO_3 filling did not cause any visible change in its structure due to the physical mixing of the two species. The diffraction peaks corresponding to MoO_3 and PEBAX 2533 occurred closely and hence coincided with each other, which resulted in broader diffraction peak at 12^o~35^o for the final composite-filled membrane.

3.2 Swelling performance of membranes

The affinity of membrane for a given chemical can be quantified by its DS (Liu et al. 2011, Mandal &Bhattacharya 2006). At room temperature, the swelling property and sorption capability of the filled membranes with different filler contents of MoO_3 (in the feed mixture) were studied, with pyrrole concentration of 2000 $\mu g \cdot g^{-1}$ and the results are compiled in **Fig. 5**. It can be seen that DS of filled membranes initially increased followed by a decrease with increasing MoO_3 microspheres filler content. The DS of filled membrane reached to maximum (an increase of 13.84%) at filler content of 4 wt.%. Further increasing the filler content led to decrease in DS. Below 4 wt.% filler contents, sorption performance increased with increasing filler content due to fact that MoO_3 particles in the membrane were well-distributed and possessed high specific surface areas (SSA) and deficient electronic structure, facilitating strong adsorption interaction with the feed mixture. This was more favorable for pyrrole having solitary electron pair, thus strongly enhanced the swelling performance of membranes. With increasing filler content, unification of particles occurred, which impeded the movement of the polymer chains in the membrane and hence reduced the number of channels for mixture feed to enter

membranes. From these results, 4 wt.% MoO_3 was chosen as the optimum filler amount for onward experiments.

The effect of temperature on the swelling properties of filled membranes was investigated at 2000 μg/g concentration of binary mixture and 4 wt.% filler contents. The results shown in **Fig. 6 (a)** suggested that DS of the filled film increased gradually with increasing temperature, and achieved maximum value of 31.25% at 70 ^{o}C. This was attributed to the increased Brownian movements of molecules in the binary mixture as well as those in polymer chain, hence facilitated better contacts and led to enhanced swelling behavior. Furthermore, the swelling resulted in increased volume of the membranes, thus increasing the free space.

We further analyzed the effect of pyrrole concentration on DS of 4 wt.% filled film and the results are picturized in **Fig. 6 (b)**, which suggested that a dramatic increase in the DS with increasing time and reached equilibrium after 30 min. The swelling equilibrium increased with increasing pyrrole concentration. At 5000 $\mu g \cdot g^{-1}$ feed liquid concentration, DS of the filled film reached 24.95%. These results revealed that membranes preferentially adsorbed pyrrole from its mixture with *n*-heptane, which can be explained by the solubility parameter theory. The solubility parameter of PEBAX2533 is 19.5 $J^{1/2}.cm^{-3/2}$, which is much closer to that of pyrrole (19.1 $J^{1/2}.cm^{-3/2}$) than that of *n*-heptane (15.3 $J^{1/2}.cm^{-3/2}$). This high selectivity of PEBAX/PAN membranes could of great potential for practical applications involving gasoline denitrification.

3.3 Pervaporation performance

3.3.1 Effect of MoO_3 loading capacity on pervaporation

The variations in total fluxes and separation factors for MoO_3 loading capacity at 30 ^{o}C and pyrrole concentration of 2000 $\mu g \cdot g^{-1}$ are shown in **Fig. 7**. It can be seen that by increasing filler content from 0 wt.% to 4 wt.%, the separation factor correspondingly increased, mainly because higher amount of MoO_3 provides more hydrogen bonds formation with pyrrole. The reversible reaction enhances the sorption selectivity of pyrrole, therefore, increasing the concentration of pyrrole in the membrane. MoO_3 endows the membrane with higher adsorption selectivity and diffusion selectivity, which result in a clear increase in the separation factors from 12 to 20 (increased by 72%). Further increase in MoO_3 content leads to agglomeration which creates non-selective defects and hinders the transport of MoO_3, ultimately leading to a decrease in separation factors. The permeation flux increases with increasing MoO_3 content up to 4 wt.%. The particles are uniformly dispersed in membranes and at lower MoO_3 filler content, the larger SSA and affinity to pyrrole contributed to the increase in permeation flux. Moreover, MoO_3 particles intervene the PEBAX matrix packing and increase the fractional free volume of the hybrid membrane, thus, decrease the diffusion resistance to permeation. However, the pathways in membrane through which the molecules permeate gets longer because of high horizontal stacks, which would decrease the permeation flux (Yang et al. 2004, Zhao &Jin 2017). Increasing filler content also leads to occupation of free space in

polymer by MoO_3 particles and reduces the free volume, which result in impeding the movement of the polymer chain in membranes.

Solution-diffusion mechanism is widely used to describe the principle of pervaporative separation (Wang et al. 2016). To better illustrate the effect of incorporated nano MoO_3 on solution and diffusion process, the sorption of penetrant molecules in the membrane was evaluated by sorption experiments. The sorption capacity of membranes in the feed solution (2000 ppm pyrrole/*n*-heptane as model gasoline feed) at 30 °C was evaluated and the results are shown in **Fig. 6 (b)**. The sorption amount of pyrrole in the membranes is much lower than that of *n*-heptane, because of its low concentration. The incorporated MoO_3 shows minor influence on the sorption capacity of the membranes towards pyrrole and *n*-heptane. The pyrrole/*n*-heptane sorption selectivity of PEBAX pristine membrane and PEBAX-MoO_3 hybrid membranes suggested that MoO_3 and PEBAX have similar affinity towards pyrrole. However, the diffusion selectivity increased by more than 50% after incorporating MoO_3 in PEBAX. Therefore, the diffusion process demonstrated a decisive effect on the enhanced permeation flux and separation factor of the hybrid membrane. The hybrid membrane can be divided into three interfaces: polymer matrix, filler and polymer-filler interface. Among the three sections, MoO_3 are impermeable to the penetrant molecules (Salmeron et al. 1982). The crystallinity of the PEBAX-MoO_3 hybrid membrane is similar to that of PEBAX pristine membrane. The fractional free volume of PEBAX-MoO_3 hybrid membrane is even smaller than that of PEBAX pristine membrane. However, the diffusion coefficients of pyrrole and *n*-heptane exhibit the opposite trends compared to the change of free volume properties. Thus, one can conclude that the increase in diffusion coefficient mainly arise from the PEBAX-MoO_3 interface. The interaction between the basal plane of MoO_3 and pyrrole molecules lies within the scope of reversible chemical complexation (King 1987), indicating that MoO_3 particles can serve as a facilitated transport carrier for pyrrole molecules via “hopping” from one carrier to another (Pinnau &Toy 2001). The large surface area of MoO_3 particles provides a continuous transport pathway for pyrrole molecules, which is quite different from the traditional isolated facilitated transport sites. The reversible reaction between pyrrole and MoO_3 particles enhances the transport rate of pyrrole in the membrane, thus endows the hybrid membrane with higher diffusion selectivity (Hong et al. 2000). After incorporating MoO_3 particles into PEBAX matrix, the continuous facilitated transport pathway on MoO_3 particles obviously enhances the diffusion coefficient of pyrrole in comparison with that of *n*-heptane, leading to increased diffusion selectivity, which consequently endows the membrane with high pyrrole selectivity.

These results indicated that the membrane with 4 wt.% filler has the best pervaporation performance, optimal total flux and separation factor of pyrrole, which is identical to the conclusion of the swelling experiments. We further applied PSI to comprehensively evaluate the parameter responsible for membrane separation performance. The data in **Fig. 8** show that PSI of 4 wt.% filler content based membranes was maximum i.e. 29.53%, which once again confirmed the results reported in earlier sections of this study.

3.3.2 Effect of feed-liquid temperature

The effect of feed-liquid temperature on pervaporation performance of 4 wt.% filled-composite membranes are shown in **Fig. 9**. At constant pyrrole concentration of 2000 μg·g^{-1}, the permeation total flux increases continuously with increasing feed-liquid temperature from 30 to 70 ^{o}C, while the separation factor decreases gradually. During the pervaporation process, the pressure difference is the primary driving force due to the fact that upstream pressure is atmospheric while the downstream pressure is kept at about 101 kPa. Additionally, increasing operating temperature exacerbates the movement of molecules, accelerating the diffusion rate, and intensifies the movement of polymer chain segments. Molecules of each component can quickly and effectively diffuse through the larger free volume of the polymer chain gap, which results in increasing the permeation flux (Qi et al. 2006). However, the separation factor decreases with increasing temperature, which may be due more sensitive nature of *n*-heptane permeation to temperature.

The sensitivity of component flux to temperature can be further reflected by the activation energy, which in turn reflects the extent to which the temperature affects the permeability of individual component (Saini et al. 2017). According to Arrhenius **Eq. (5)** (Pan et al. 2018), as shown in **Fig. 10**, the osmotic activation energy of pyrrole and *n*-heptane are 6.61 kJ·mol^{-1} and 15.59 kJ·mol^{-1}, respectively. Compared with pyrrole, the effect of temperature change on *n*-heptane flux is more significant. As the feed temperature rises, the permeation flux of *n*-heptane increases more pronouncedly, while the affinity of membrane for pyrrole weakens, and *n*-heptane molecules pass through the membrane more easily, which decreases the separation factor. This conclusion is consistent with the results of **Fig. 10**.

$$J_i = A_i e^{-\frac{E_i}{RT}} \qquad (5)$$

Where, J_i is the permeation flux of component *i*, kgm^{-2}h^{-1}. A_i is the pre-exponential factor of component *i*, kgm^{-2}h^{-1}. E_i is the permeation activation energy of component *i*, kJ·mol^{-1}. T is the absolute temperature; K. *R* is the molar gas constant, 8.314 J×mol×K^{-1}.

3.3.3 Effect of feed concentration

The effect of pyrrole feed concentrations on total flux and separation factor are shown in **Fig. 11**. At 70 ^{o}C feed-liquid temperature and increasing pyrrole concentration in feed from 1000 to 5000 ppm, the permeation flux and separation factors increased continuously. The total flux increased from 2.23 to 3.12 kgm^{-2}h^{-1} corresponding to an increase of 39.91%, while the separation factors enhanced from 15.65 to 19.76. The enhanced total fluxes further confirmed the results of swelling experiments. Previous swelling experiments showed that higher concentration could increase the DS of membranes, thus weakening the interaction between the polymer chains, which in turn provides more free space in the membrane for molecules for feed liquid in penetrating the membrane, thus increasing the permeation flux. As pyrrole is a weak polar molecule with Lewis-base, thus MoO_3 particles exhibit strong affinity for it (Mandal &Bhattacharya 2006, Yang et al. 2012). Upon increasing pyrrole concentration in feed liquid, more pyrrole

molecules dissolve and diffuse into the membrane, which desorb downstream, thus leading to increase in separation factor.

3.4. Mechanism of the Pervaporative Denitrogenation of Pyrrole/n-heptane

Fig. 12 shows the mechanism of pyrrole molecules being a weak base once interacts with MoO_3 Lewis-acid particles in n-heptane solvent via PEBAX/PAN membranes. As discussed above, increase in pyrrole concentration increases the affinity of MoO_3 species hence increases permeation ability. MoO_3 losses its electron while in contact with the pyrrole species by oxidizing to Mo^{6+}. The oxidized MoO_3 then reduces by adsorbing to the polymer metrics. Where the pyrrole molecules dissolve and diffuse into the membrane, which desorb downstream, thus leading to increase in separation factor.

4. Conclusions

In summary, MoO_3-PEBAX/PAN filled-composite membrane was prepared using MoO_3 as filler. The swelling and pervaporation properties of the prepared membranes in the pyrrole/*n*-heptane system as model fuel oil were investigated. Results showed that higher concentration of pyrrole facilitated better swelling performance of the membrane due to their higher mutual affinity. The permeation flux and separation factor of the membrane increased with increasing pyrrole concentration but declined with increasing operating temperature. Pervaporation experiments revealed that at 4 wt.% MoO_3 contents, membrane showed the best comprehensive separation performance. When the feed temperature is 30 ^{o}C and 5000 $\mu g \cdot g^{-1}$ feed concentration, the total permeation flux and separation factored reached to 3.12 $kg \bullet m^{-2} \bullet h^{-1}$ and 19.76 respectively. This study attributed to the ease of synthesis, cost effectiveness and high efficiency of the proposed PEBAX/PAN filled-composite membrane, could be envisaged of potential interest for industrial applications involving denitrification of fuel oils.

Declarations

Nomenclature

A	effective area of membrane (cm^2)
DS	swelling degree (%)
E_{pi}	activation energy of permeate for component i ($kJ \cdot mol^{-1}$)
J	total permeation flux ($kg \cdot m^{-2} \cdot h^{-1}$)
J	partial permeation flux ($kg \cdot m^{-2} \cdot h^{-1}$)
J_o	pre-exponential factor
T	operating time (h)
T	feed absolute temperature (K)
W_d	mass of dry membrane (g)
W_w	mass of wet membrane (g)
X	mass fraction of component in feed (wt.%)
Y	mass fraction of component in permeate (wt.%)
Δ	solubility parameter ($J^{1/2} \cdot cm^{-3/2}$)
A	separator factor

Ethics approval and consent to participate

The materials used in this study and the strategies followed in designing the system do not harm any living or non-living creature, both directly or indirectly, hence obeys all the ethical values.

Secondly, the research is conducted in the abovementioned laboratory with high accuracy and originality. The data has also not been submitted to this journal before, or to any other journal in parts or as whole.

Therefore, the consent of participation to the journal by the authors is ethically approved.

Consent for publication

We the authors of the manuscript hereby transfer all the copy rights to the Environmental Science and Pollution Research under the helm of Springer.

Availability of data and materials

All data generated or analysed during this study are included in this published article [and its supplementary information files].

Competing interests

The authors Liu Kun, Yu Qiulan, Muhammad Yaseen, and Sidra Subhan declare that they have no known competing financial interests or personal relationships that could have appeared to influence the work reported in this paper.

The work was funded by Guangxi Provincial Key Laboratory of Petrochemical Resource Processing and Process Intensification Technology (2013Z009); Guangxi Natural Science Foundation (2014jj AA20079).

Author's contribution

Dr. Kun Liu: Funding acquisition and supervison.

Ms. Yu Qiulan: Experimental work, draft writing.

Dr. Muhammad Yaseen: Project designing and data analysis.

Dr. Sidra Subhan: Data analysis, writing and editing.

Acknowledgement

This work was supported by Guangxi Provincial Key Laboratory of Petrochemical Resource Processing and Process Intensification Technology (2013Z009); Guangxi Natural Science Foundation (2014jj AA20079).

References

Abdul-quadir MS, van der Westhuizen R, Welthagen W, Ferg EE, Tshentu ZR, Ogunlaja AS (2018): Adsorptive denitrogenation of fuel over molecularly imprinted poly-2-(1H-imidazol-2-yl)-4-phenol microspheres. New Journal of Chemistry 42, 13135-13146

Adams J, Giam CSJEs, technology (1984): Polynuclear azaarenes in wood preservative wastewater. 18, 391-394

Ali MF, Al-Malki A, El-Ali B, Martinie G, Siddiqui MNJF (2006): Deep desulphurization of gasoline and diesel fuels using non-hydrogen consuming techniques. 85, 1354-1363

Amaral R, Habert A, Borges CJML (2014): Activated carbon polyurethane membrane for a model fuel desulfurization by pervaporation. 137, 468-470

Ammar SH, Kareem YS, Mohammed MS (2020): Catalytic-oxidative/adsorptive denitrogenation of model hydrocarbon fuels under ultrasonic field using magnetic reduced graphene oxide-based phosphomolybdic acid (PMo-Fe3O4/rGO). Ultrasonics Sonochemistry 64, 105050

Balko J, Glaser R, Wormsbecher R, Wynn N (2002): Reduce your Tier 2 gasoline sulfur compliance costs with Grace Davison S-Brane technology, NPRA Annual Meeting, AM-02-21

Busca GJI, Research EC (2009): Bases and basic materials in industrial and environmental chemistry: a review of commercial processes. 48, 6486-6511

Castro-Muñoz R (2019): Pervaporation: The emerging technique for extracting aroma compounds from food systems. Journal of Food Engineering 253, 27-39

Chen J, Li J, Qi R, Ye H, Chen CJAb, biotechnology (2010): Pervaporation separation of thiophene–heptane mixtures with polydimethylsiloxane (PDMS) membrane for desulfurization. 160, 486-497

Dorbon M, Bernasconi CJF (1989): Nitrogen compounds in light cycle oils: identification and consequences of ageing. 68, 1067-1074

Escola J, Aguado J, Serrano D, Briones L, Díaz de Tuesta J, Calvo R, Fernandez EJE, Fuels (2012): Conversion of polyethylene into transportation fuels by the combination of thermal cracking and catalytic hydroreforming over Ni-supported hierarchical beta zeolite. 26, 3187-3195

Gao J, Mao H, Jin H, Chen C, Feldhoff A, Li Y (2020): Functionalized ZIF-7/Pebax® 2533 mixed matrix membranes for CO2/N2 separation. Microporous and Mesoporous Materials 297, 110030

Hong SU, Jin JH, Won J, Kang YSJAM (2000): Polymer–salt complexes containing silver ions and their application to facilitated olefin transport membranes. 12, 968-971

Huang J, Meagher MJJoMS (2001): Pervaporative recovery of n-butanol from aqueous solutions and ABE fermentation broth using thin-film silicalite-filled silicone composite membranes. 192, 231-242

Huang T-C, Liu Y-C, Lin G-S, Lin C-H, Liu W-R, Tung K-L (2020): Fabrication of pebax-1657-based mixed-matrix membranes incorporating N-doped few-layer graphene for carbon dioxide capture enhancement. Journal of Membrane Science 602, 117946

King CJJHospt (1987): Separation processes based on reversible chemical complexation. Wiley: New York, pp. 760-774

Laredo GC, Likhanova NV, Lijanova IV, Rodriguez-Heredia B, Castillo JJ, Perez-Romo P (2015): Synthesis of ionic liquids and their use for extracting nitrogen compounds from gas oil feeds towards diesel fuel production. Fuel Processing Technology 130, 38-45

Le NL, Wang Y, Chung T-SJJoMS (2011): Pebax/POSS mixed matrix membranes for ethanol recovery from aqueous solutions via pervaporation. 379, 174-183

Li Y, Liu D, Liu CJE, Fuels (2009): Hydrodesulfurization (HDS) and hydrodenitrogenation (HDN) performance of an ex situ presulfided MoNiP/Al2O3 catalyst: model compounds study and pilot test for fluidized catalytic cracking (FCC) diesel oil. 24, 789-795

Lin L, Wang G, Qu H, Yang J, Wang Y, Shi D, Kong YJJoms (2006): Pervaporation performance of crosslinked polyethylene glycol membranes for deep desulfurization of FCC gasoline. 280, 651-658

Lin L, Kong Y, Xie K, Lu F, Liu R, Guo L, Shao S, Yang J, Shi D, Zhang YJS, Technology P (2008): Polyethylene glycol/polyurethane blend membranes for gasoline desulphurization by pervaporation technique. 61, 293-300

Lin L, Zhang Y, Kong YJF (2009): Recent advances in sulfur removal from gasoline by pervaporation. 88, 1799-1809

Liu K, Fang CJ, Li ZQ, Fan FF, Han JJ (2013): Removal of Thiophene from Binary Mixtures Using Polyether Block Amide (PEBAX) Film by Pervaporation, Advanced Materials Research. Trans Tech Publ, pp. 4101-4108

Liu W, Li B, Cao R, Jiang Z, Yu S, Liu G, Wu HJJoms (2011): Enhanced pervaporation performance of poly (dimethyl siloxane) membrane by incorporating titania microspheres with high silver ion loading. 378, 382-392

Mandal MK, Bhattacharya PJJoms (2006): Poly (ether-block-amide) membrane for pervaporative separation of pyridine present in low concentration in aqueous solution. 286, 115-124

Mapiour M, Sundaramurthy V, Dalai A, Adjaye JJF (2010): Effects of the operating variables on hydrotreating of heavy gas oil: Experimental, modeling, and kinetic studies. 89, 2536-2543

Marani D, Silva RH, Dankeaw A, Norrman K, Werchmeister RML, Ippolito D, Gudik-Sørensen M, Hansen KK, Esposito V (2017): NOx selective catalytic reduction (SCR) on self-supported V–W-doped TiO2 nanofibers. New Journal of Chemistry 41, 3466-3472

McKay J, Weber J, Latham DJAC (1976): Characterization of nitrogen bases in high-boiling petroleum distillates. 48, 891-898

Merkel TC, Blanc R, Ciobanu I, Firat B, Suwarlim A, Zeid JJJoms (2013): Silver salt facilitated transport membranes for olefin/paraffin separations: Carrier instability and a novel regeneration method. 447, 177-189

Mojaverian Kermani A, Ahmadpour A, Rohani Bastami T, Ghahramaninezhad M (2018): Deep oxidative desulfurization of dibenzothiophene with {Mo132} nanoballs supported on activated carbon as an

efficient catalyst at room temperature. New Journal of Chemistry 42, 12188-12197

Mortaheb HR, Ghaemmaghami F, Mokhtarani BJCER, Design (2012): A review on removal of sulfur components from gasoline by pervaporation. 90, 409-432

Muhammad Y, Rahman AU, Rashid HU, Sahibzada M, Subhan S, Tong Z (2019a): Hydrodesulfurization of dibenzothiophene using Pd-promoted Co–Mo/Al2O3 and Ni–Mo/Al2O3 catalysts coupled with ionic liquids at ambient operating conditions. RSC Advances 9, 10371-10385

Muhammad Y, Rashid HU, Subhan S, Rahman AU, Sahibzada M, Tong Z (2019b): Boosting the hydrodesulfurization of dibenzothiophene efficiency of Mn decorated (Co/Ni)-Mo/Al2O3 catalysts at mild temperature and pressure by coupling with phosphonium based ionic liquids. Chemical Engineering Journal 375, 121957

Nunes MAG, Mello PA, Bizzi CA, Diehl LO, Moreira EM, Souza WF, Gaudino EC, Cravotto G, Flores EMM (2014): Evaluation of nitrogen effect on ultrasound-assisted oxidative desulfurization process. Fuel Processing Technology 126, 521-527

Oliveira EC, de Campos MClV, Lopes ASA, Vale MGR, Caramão EBJJoCA (2004): Ion-exchange resins in the isolation of nitrogen compounds from petroleum residues. 1027, 171-177

Pan F, Wang M, Ding H, Song Y, Li W, Wu H, Jiang Z, Wang B, Cao XJJoms (2018): Embedding Ag+@ COFs within Pebax membrane to confer mass transport channels and facilitated transport sites for elevated desulfurization performance. 552, 1-12

Pinnau I, Toy LGJJoMS (2001): Solid polymer electrolyte composite membranes for olefin/paraffin separation. 184, 39-48

Qi R, Wang Y, Li J, Zhao C, Zhu SJJoMS (2006): Pervaporation separation of alkane/thiophene mixtures with PDMS membrane. 280, 545-552

Qu H, Kong Y, Lv H, Zhang Y, Yang J, Shi DJCEJ (2010): Effect of crosslinking on sorption, diffusion and pervaporation of gasoline components in hydroxyethyl cellulose membranes. 157, 60-66

Rahman NAA, Fermoso J, Sanna A (2018): Effect of Li-LSX-zeolite on the in-situ catalytic deoxygenation and denitrogenation of Isochrysis sp. microalgae pyrolysis vapours. Fuel Processing Technology 173, 253-261

Saini A, Jat SK, Shekhawat DS, Kumar A, Dhayal V, Agarwal DCJMRB (2017): Oxime-modified aluminium (III) alkoxides: potential precursors for γ-alumina nano-powders and optically transparent alumina film. 93, 373-380

Salmeron M, Somorjai G, Wold A, Chianelli R, Liang KJCPL (1982): The adsorption and binding of thiophene, butene and H2S on the basal plane of MoS2 single crystals. 90, 105-107

Sampranpiboon P, Jiraratananon R, Uttapap D, Feng X, Huang RJJoMS (2000): Pervaporation separation of ethyl butyrate and isopropanol with polyether block amide (PEBA) membranes. 173, 53-59

Song C, Li R, Fan Z, Liu Q, Zhang B, Kitamura Y (2020): CO2/N2 separation performance of Pebax/MIL-101 and Pebax /NH2-MIL-101 mixed matrix membranes and intensification via sub-ambient operation. Separation and Purification Technology 238, 116500

Subhan S, Muhammad Y, Sahibzada M, Subhan F, Tong Z (2019a): Studies on the Selection of a Catalyst–Oxidant System for the Energy-Efficient Desulfurization and Denitrogenation of Fuel Oil at Mild Operating Conditions. Energy & Fuels 33, 8423-8439

Subhan S, Ur Rahman A, Yaseen M, Ur Rashid H, Ishaq M, Sahibzada M, Tong Z (2019b): Ultra-fast and highly efficient catalytic oxidative desulfurization of dibenzothiophene at ambient temperature over low Mn loaded Co-Mo/Al2O3 and Ni-Mo/Al2O3 catalysts using NaClO as oxidant. Fuel 237, 793-805

Sun Y, Ren S, Hou Y, Zhang K, Wu W (2018): Absorption of nitric oxide in simulated flue gas by a metallic functional ionic liquid. Fuel Processing Technology 178, 7-12

Wang Q, Li N, Bolto B, Hoang M, Xie ZJD (2016): Desalination by pervaporation: A review. 387, 46-60

Wu C, Xu TJECE Organic/Inorganic Hybrid Membranes: Overview and Perspective. 119

Yang C, Smyrl WH, Cussler EJJoMS (2004): Flake alignment in composite coatings. 231, 1-12

Yang Z, Zhang W, Li J, Chen JJS, technology p (2012): Polyphosphazene membrane for desulfurization: Selecting poly [bis (trifluoroethoxy) phosphazene] for pervaporative removal of thiophene. 93, 15-24

Yildirim AE, Hilmioglu ND, Tulbentci SJD (2008): Separation of benzene/cyclohexane mixtures by pervaporation using PEBA membranes. 219, 14-25

Yu H, Li S, Jin GJE, Fuels (2010): Catalytic hydrotreating of the diesel distillate from Fushun shale oil for the production of clean fuel. 24, 4419-4424

Zhao J, Jin WJCjoce (2017): Manipulation of confined structure in alcohol-permselective pervaporation membranes. 25, 1616-1626

Zi LYGJAPS (1996): MOLECULAR DIMENSION AND SHAPE SELECTIVITY OF ZEOLITE MOLECULAR SIEVES [J]. 3

Figures

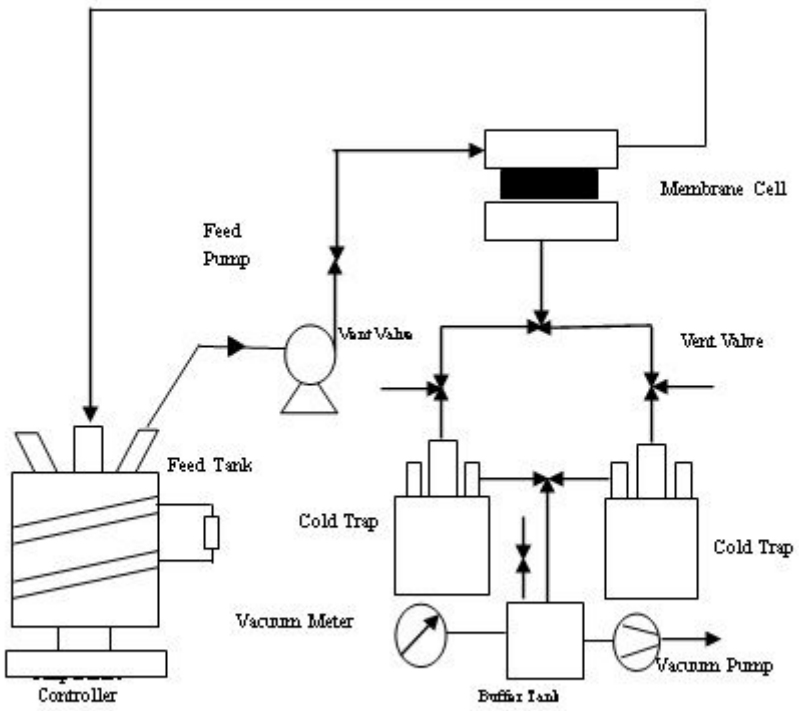

Figure 1

Schematic representation of pervaporation experimental set up.

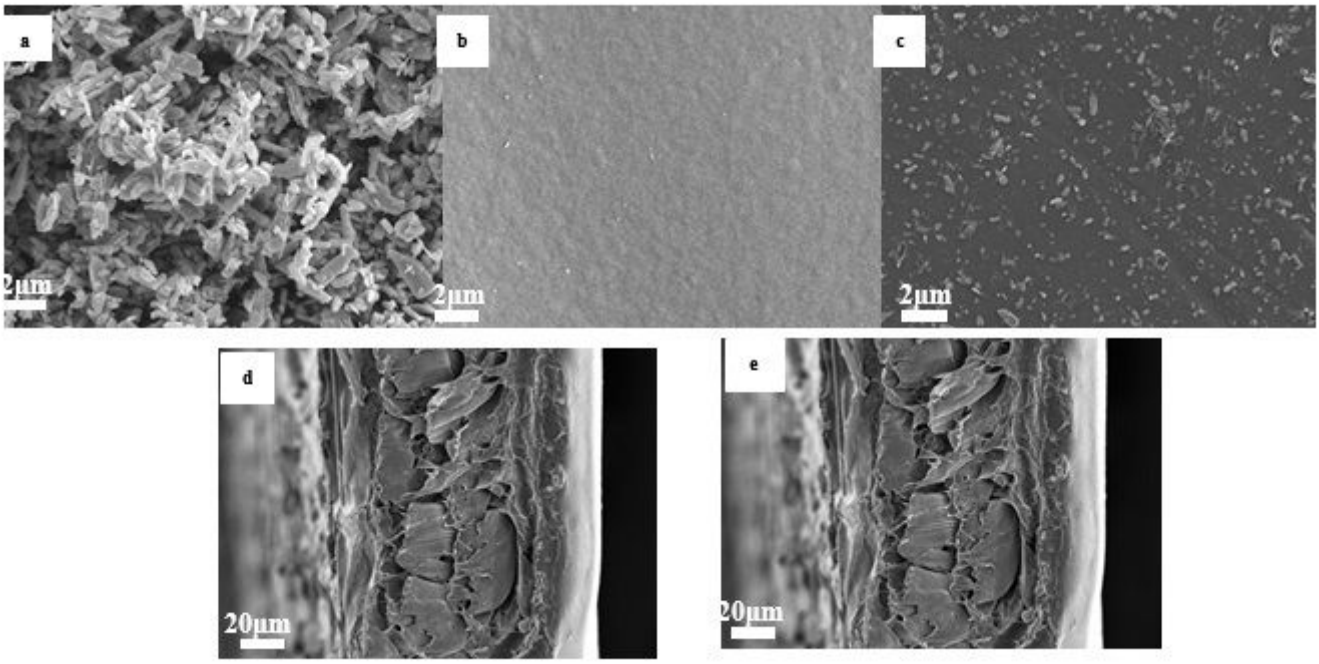

Figure 2

SEM micrographs of different membranes (a) morphology of MoO3 microspheres (b) surface of composite membrane (c) surface of composite-filled membrane (d) cross-section of composite membrane and (e) cross-section of composite-filled membrane

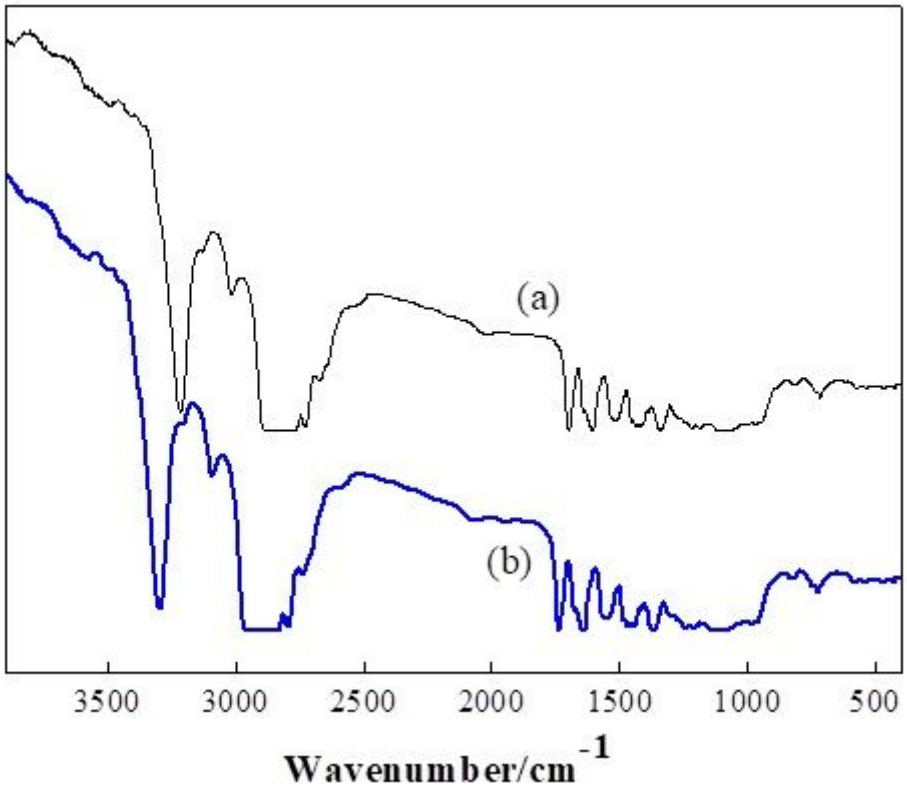

Figure 3

FT-IR Spectra of: (a) PEBAX composite membrane and (b) MoO3 filled PEBAX composite membrane

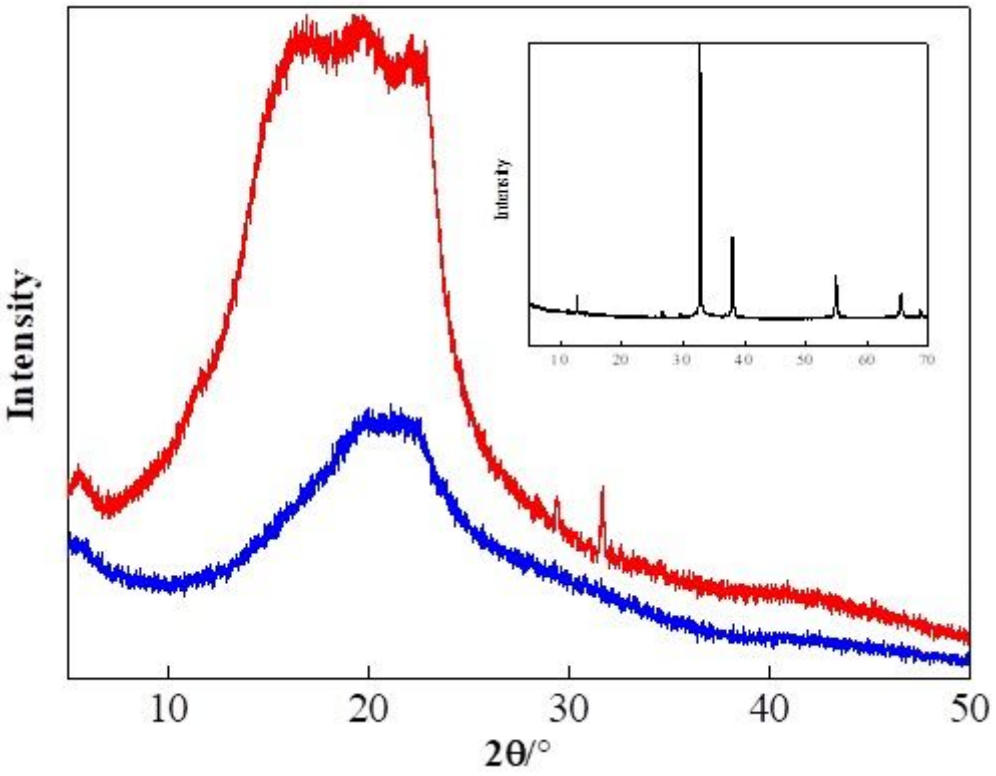

Figure 4

XRD spectra of (blue) PEBAX composite membrane and (red) MoO3 filled PEBAX composite membrane

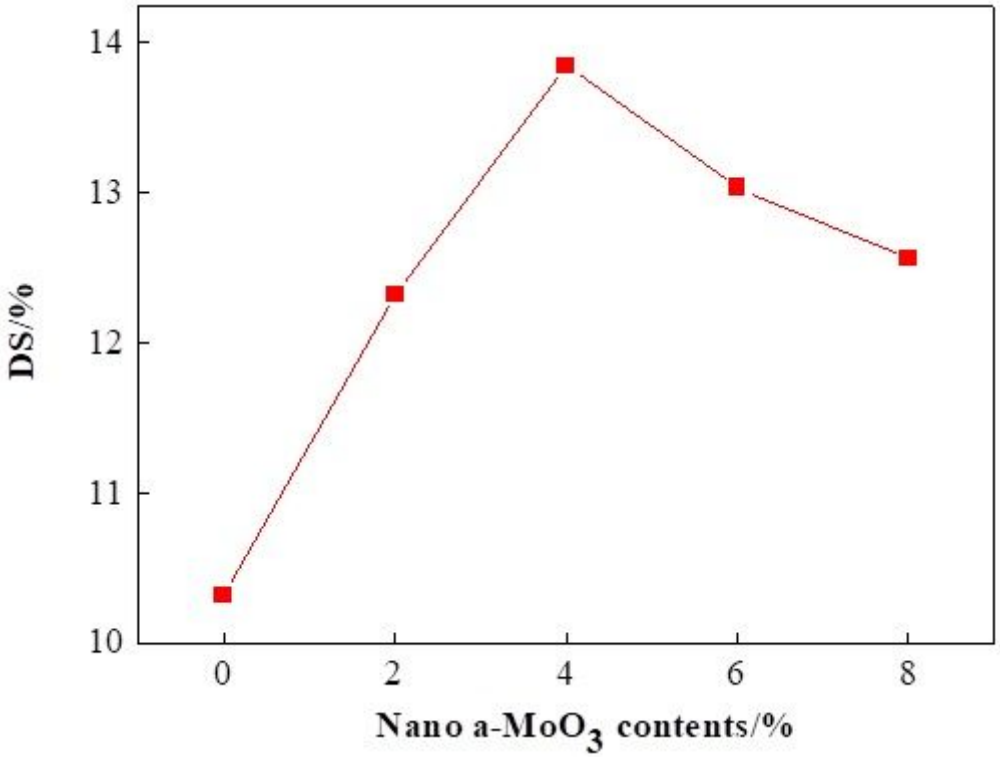

Figure 5

Effects of filler contents on swelling degree of membranes (T=30 oC, C=2000 μg×g-1)

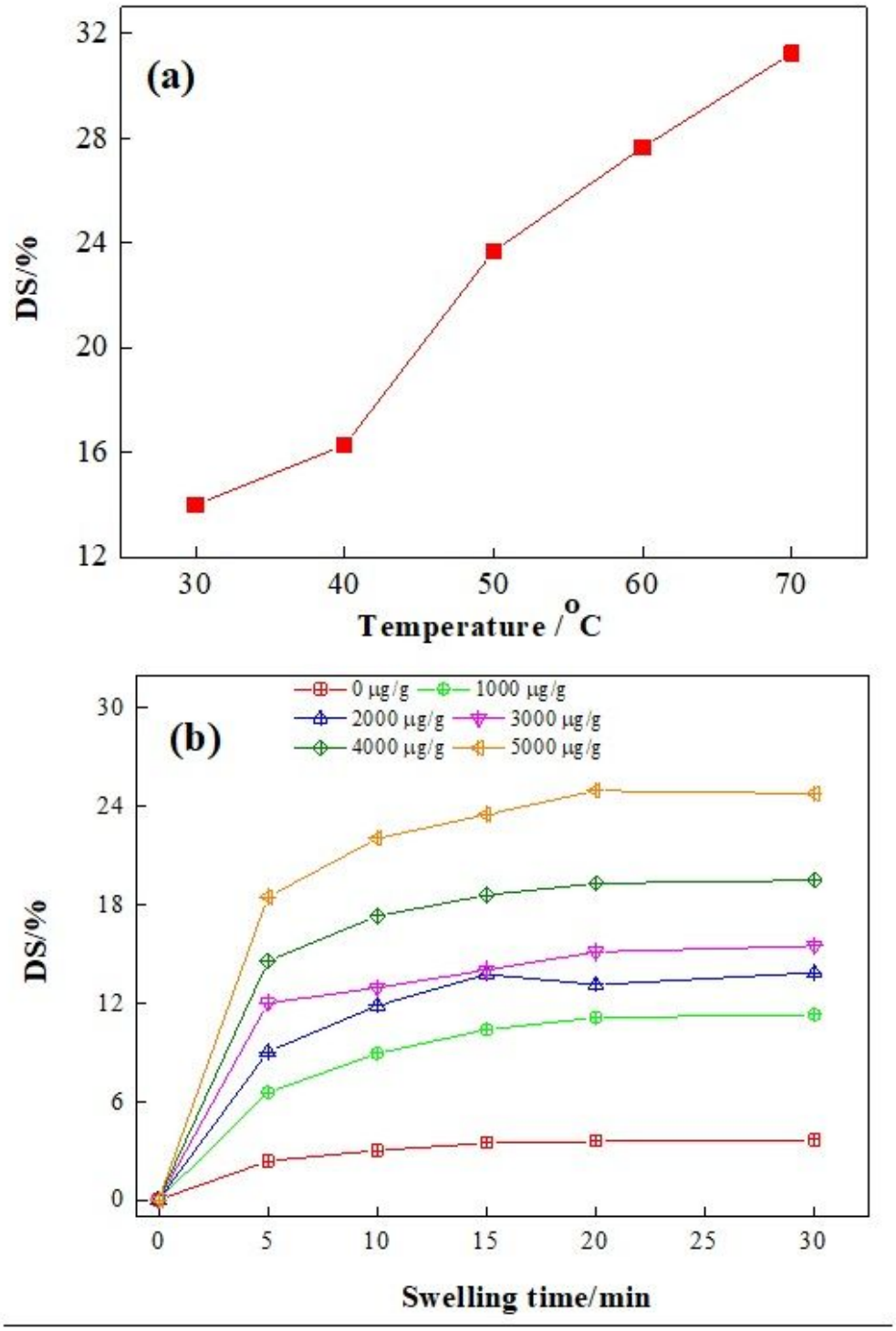

Figure 6

Effects of feed temperature on swelling degree of the 4 wt.% filled membrane (C=3000 μg×g-1) (a); swelling degree of 4 wt.% filled membrane under different feed concentrations and immersion times (T=30°C) (b).

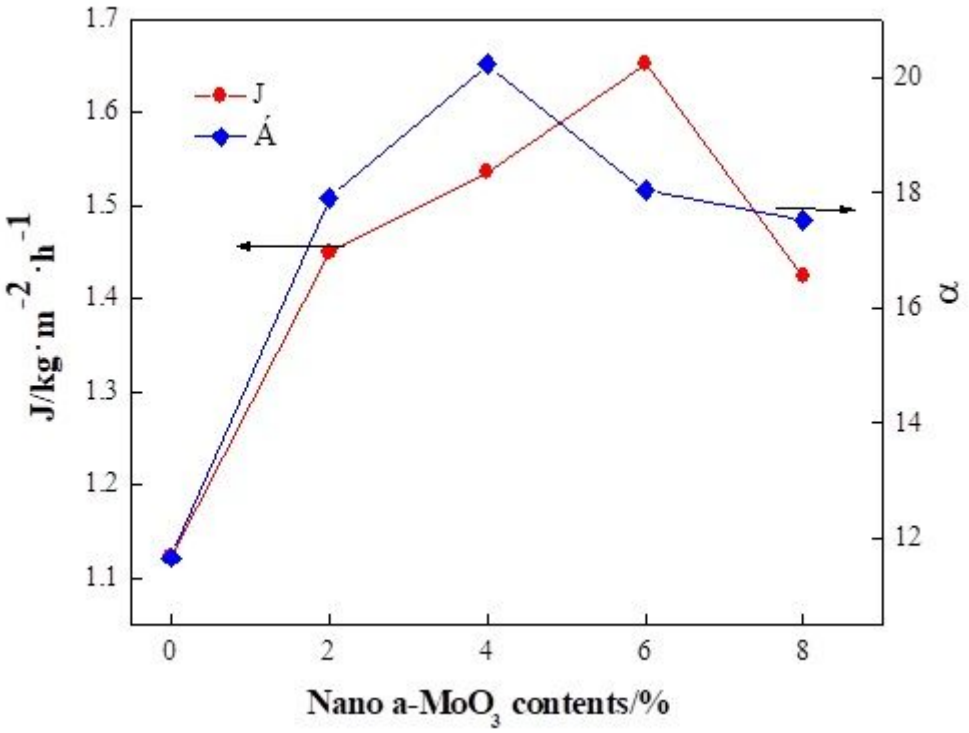

Figure 7

Effects of filler contents on pervaporation performance of the membrane (T=30°C, C=3000 μg×g-1)

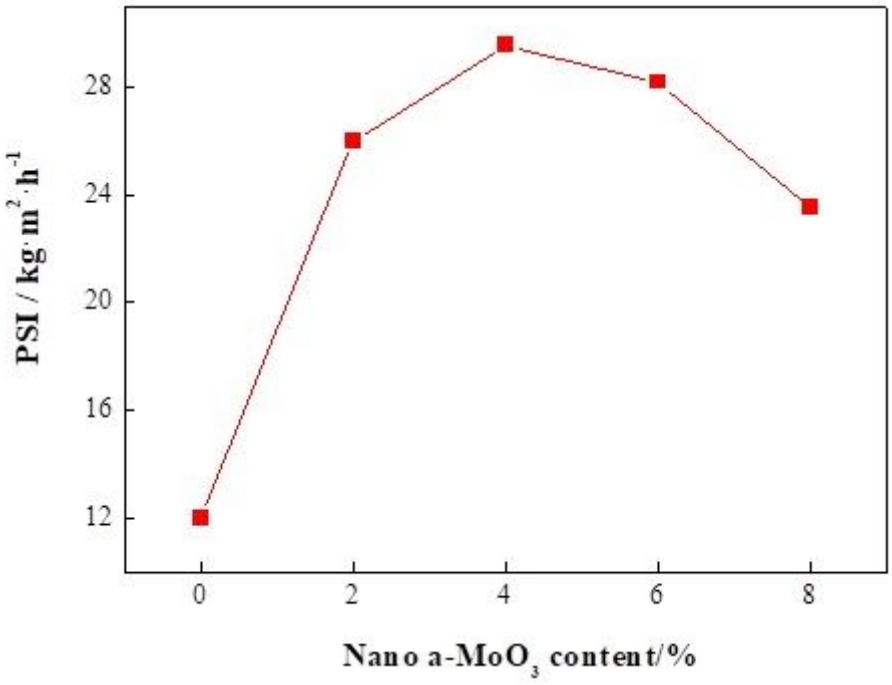

Figure 8

Profile of pervaporation separation index as a function of filler content (T=30 oC, C=3000 μg×g-1)

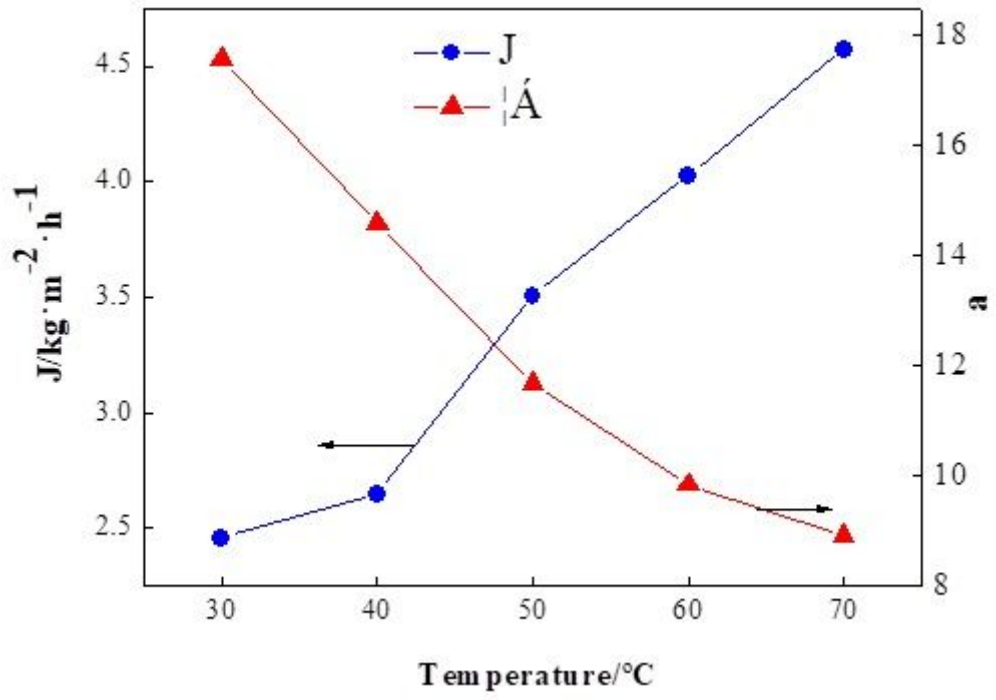

Figure 9

Effect of feed temperature on pervaporation separation performance of the 4 wt.% composite-filled membrane (C=2000μg×g-1)

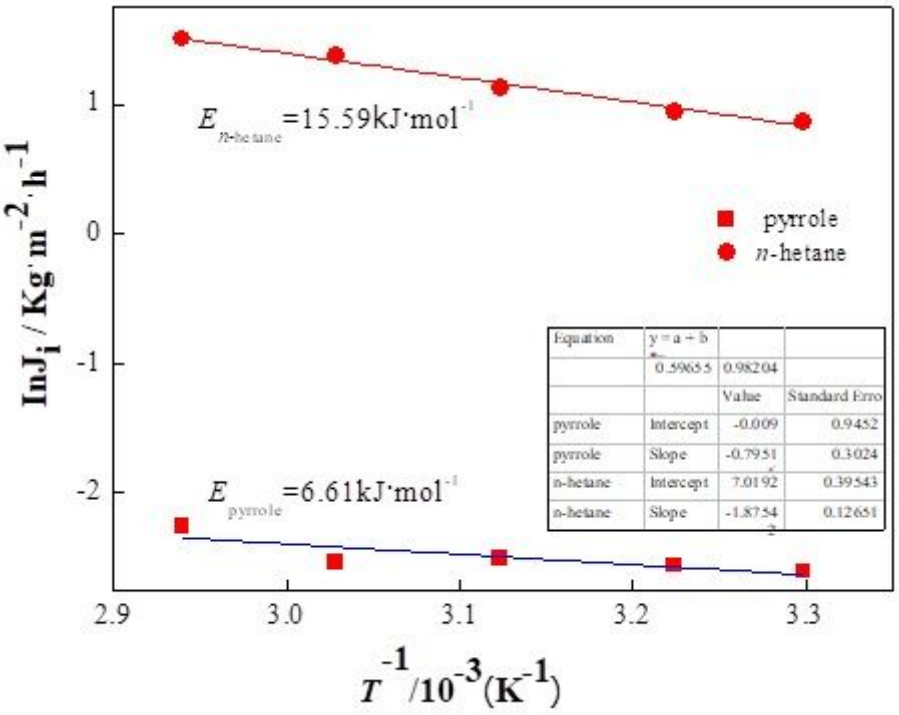

Figure 10

Arrhenius plots between the partial flux and operation temperature

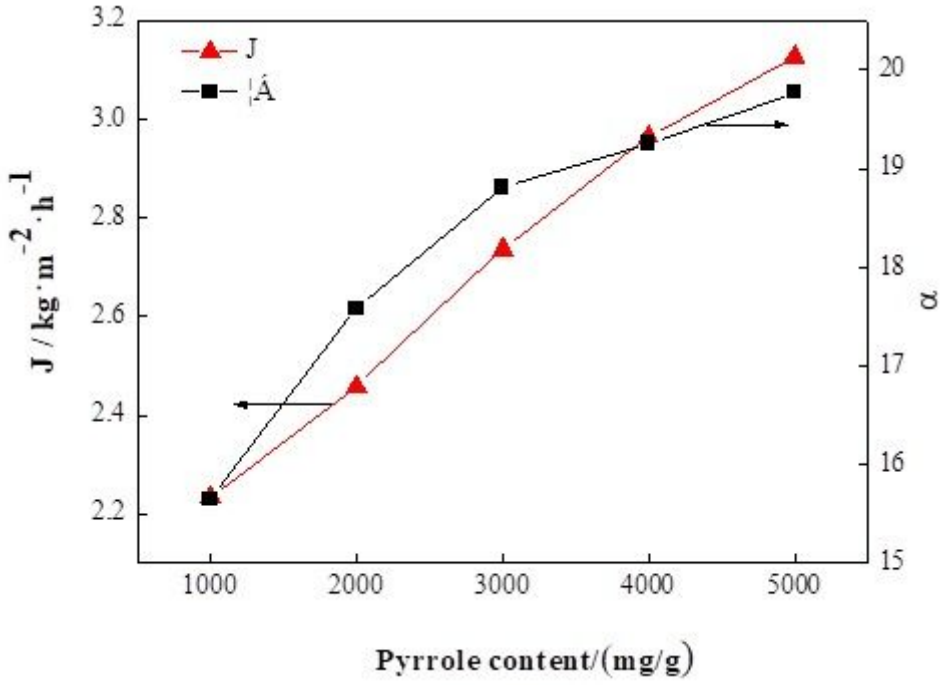

Figure 11

Effect of feed concentration on pervaporation separation performance of the 4 wt.% composite-filled membrane (T=30 oC)

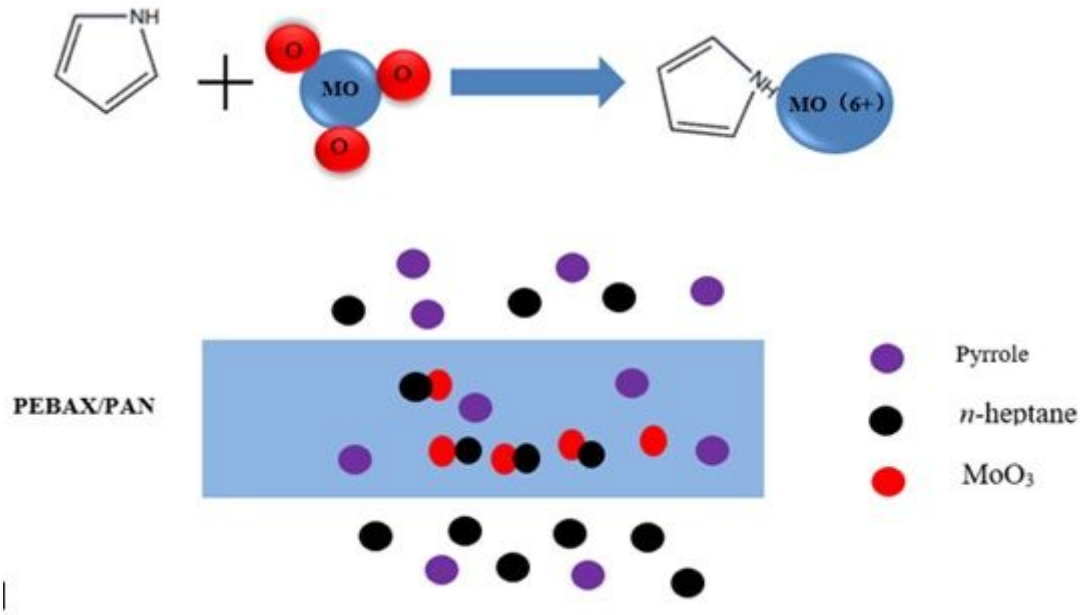

Figure 12

Mechanism of the Pervaporative Denitrogenation of Pyrrole/n-heptane

Supplementary Files

This is a list of supplementary files associated with this preprint. Click to download.

- GraphicalAbstract.pdf